JACS JOURNAL OF THE AMERICAN CHEMICAL SOCIETY
pubs.acs.org/JACS Article

Unraveling the Reaction Mystery of Li and Na with Dry Air

Yuqi Li,○ Qiunan Liu,○ Siyuan Wu, Lin Geng, Jelena Popovic, Yu Li, Zhao Chen, Haibo Wang, Yuqi Wang, Tao Dai, Yang Yang, Haiming Sun, Yaxiang Lu,* Liqiang Zhang, Yongfu Tang, Ruijuan Xiao,* Hong Li, Liquan Chen, Joachim Maier, Jianyu Huang,* and Yong-Sheng Hu*

Cite This: J. Am. Chem. Soc. 2023, 145, 10576−10583 Read Online

ABSTRACT: Li and Na metals with high energy density are promising in application in rechargeable batteries but suffer from degradation in the ambient atmosphere. The phenomenon that in terms of kinetics, Li is stable but Na is unstable in dry air has not been fully understood. Here, we use *in situ* environmental transmission electron microscopy combined with theoretical simulations and reveal that the different stabilities in dry air for Li and Na are reflected by the formation of compact Li_2O layers on Li metal, while porous and rough Na_2O/Na_2O_2 layers on Na metal are a consequence of the different thermodynamic and kinetics in O_2. It is shown that a preformed carbonate layer can change the kinetics of Na toward an anticorrosive behavior. Our study provides a deeper understanding of the often-overlooked chemical reactions with environmental gases and enhances the electrochemical performance of Li and Na by controlling interfacial stability.

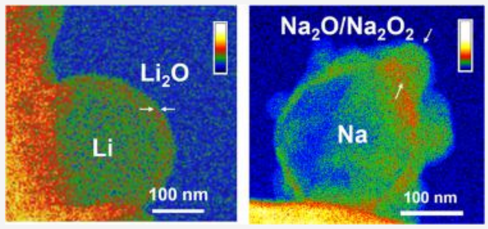

■ INTRODUCTION

The invention of Li-ion batteries promises a greener future with more electrification and less carbon emission.[1] Considering the need for future powerful devices, classic electrodes such as graphite may not satisfy the stringent requirements in terms of the energy density of batteries.[2] The use of Li metal is considered a solution to achieve high energy density on the anode side in Figure 1a, which is particularly important for Li−air, Li−sulfur, and solid-state Li batteries.[3] Li metal is highly unstable in humid air, while its relatively high air stability in a dry room enables the possibility of mass manufacturing of Li-metal batteries.[4−6] However, the application of Na metal as a promising anode for cost-effective and sustainable Na-based batteries for grid storage is hindered by its high air sensitivity even in a dry room.[7] Both alkali metals naturally have a high tendency to form oxides,[8] with Na possessing the lower ionization energy owing to the larger size, but, in turn, the smaller size of Li results in higher lattice energy of Li_2O (when compared to Na_2O), rendering Li-oxidation thermodynamically more favorable.[9] As current research mainly focuses on the electrochemical reactions in metal−air batteries, and the complex interactions of the bare metal in even dry air are not appropriately considered, the kinetic differences in the behavior of the two alkaline metals are far from being understood (cf. Figure 1b). It has to be noticed that the contact between Li or Na and the environmental gases during production and transportation processes constitutes the initial formation of solid electrolyte interphase (SEI) formation, thus setting the initial conditions for the subsequent electrochemical and chemical corrosion reactions in battery systems.[10] Thus, there is an urgent need to elucidate the interfacial passivation chemistry of alkali metals in dry air from the viewpoint of the safety and stability of alkali metal anode-based batteries, which is the focus of this work.

■ RESULTS AND DISCUSSION

Micron-Scale Characterizations of the Li/Na-Dry Air Reactions. Figure 1c shows the macroscopic changes of fresh Li and Na placed in an actual dry room (∼0% RH) for battery manufacture. After dry air exposure for 20 min, it can be seen that there is almost no color change for Li, but the surface of Na loses its shine (the products are denoted as A-Li and A-Na, respectively). The *ex situ* observation by the metallurgical microscope indicates that the metallic stripes of A-Li still exist (Figure 1d,e), whilst there is a dark coverage on A-Na in dry air (Figure 1f,g). Scanning electron microscopy (SEM) images show that the surface of A-Li is smooth with several tiny corrosion spots in Figure 1h−j. This is in contrast to A-Na, where a manifold of randomly distributed cracks with widths of 1−2 μm (Figures 1k−m and S1) are observed. Evidently, air can continuously penetrate into the cracks and react with the inner fresh Na. Atomic force microscopy (AFM) detects that the surface of A-Na has a larger roughness than that of A-Li in Figures 1m,o and S2. Microscopically, the passivation layer of

Received: December 24, 2022
Published: May 2, 2023

https://doi.org/10.1021/jacs.2c13589
J. Am. Chem. Soc. 2023, 145, 10576−10583

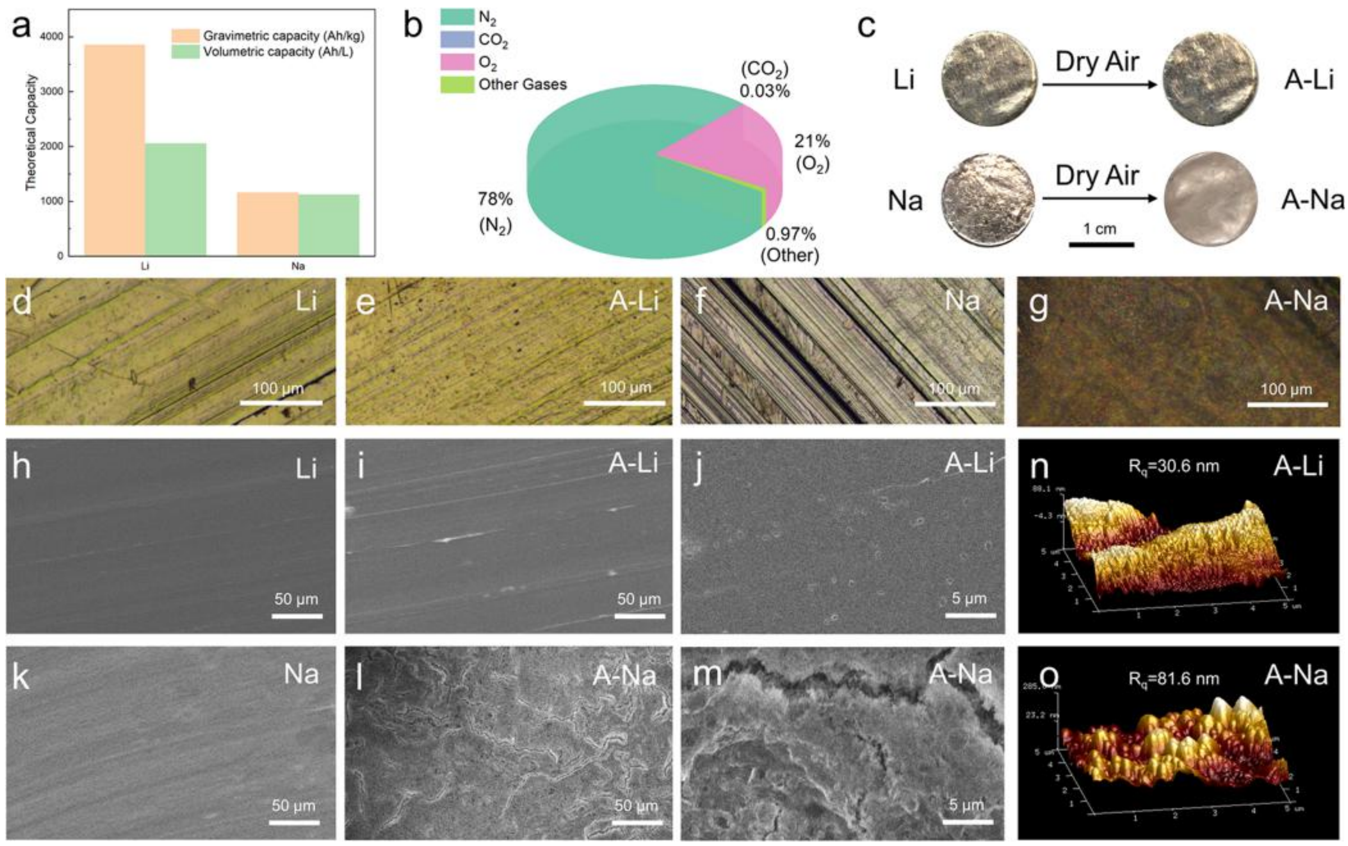

Figure 1. Micron-scale investigation of the surface layer of Li and Na in dry air. (a) Theoretical capacity of metallic Li and Na. (b) Schematic of air composition. (c) Digital images of Li, A-Li, Na, and A-Na (A-Li/Na is the product of Li/Na after dry air exposure for 20 min). (d−g) *Ex situ* optical microscopy images of Li, A-Li, Na, and A-Na. (h−m) *Ex situ* scanning electron microscopy (SEM) images of Li, A-Li, Na, and A-Na. Note that the *ex situ* observations of optical microscopy and SEM are quasi in situ ones achieving observation for the same position after air contact. (n, o) Atomic force microscopy (AFM) images of A-Li and A-Na. The values of R_q represent the roughness of A-Li and A-Na.

A-Na with a relatively large surface area can capture more air than that of A-Li. Further X-ray photoelectron spectroscopy (XPS) and time-of-flight secondary-ion mass spectrometry (ToF-SIMS) analyses in Figures S3−S5 show that an inorganic bilayer with an outer carbonate layer and an inner oxide layer is formed on both A-Li and A-Na, but the spatial distribution of these two layers is much more distinct, e.g., the carbonate layer is suggested to be thicker on A-Na than that on A-Li.

In situ environmental transmission electron microscopy (ETEM) observations are carried out to obtain detailed microscopic information. Li or Na metal particles (Figures 2a,f and S6), which are *in situ* generated in specially built solid-state batteries under high vacuum, can be considered as proper model materials to investigate.[11] As 1 mbar dry air flows into the ETEM chamber, the morphology of Li is almost unchanged but a void emerges in the interior of Na after about 3 h. The rapid loss of inner Na can be attributed to the Kirkendall effect arising from the huge difference between inward and outward mass diffusion[12] due to the faster migration of Na^+ than that of O^{2-}. This is the first observation of such an effect in the Na system. Dry air noticeably thickens the passivation layer of Na, which exhibits a rough and loose morphology in Figure 2g,h. However, the thickness of the passivation layer of Li only slightly increases, keeping a thin and flat surface (Figure 2b). The electron diffraction pattern (EDP) and electron energy-loss spectroscopy (EELS) results show that for the Li system, its inner core is metallic Li, while its shell consists of Li_2CO_3/Li_2O with poor crystallinity and small grain sizes (Figure 2c−e). As for the Na system, the Na_2CO_3 shell with high crystallinity (many spots and rings from EDP in Figure 2i−k) covers the core of Na. The absence of a Na_2O signal suggests a thick Na_2CO_3 layer.

Furthermore, different gases including O_2, N_2, and CO_2 are separately injected into the chamber. First, under an O_2 environment, ETEM captures a rapid formation of a homogeneous and thin passivation layer on Li (Figure 2l−n), whose thickness varies from 4 to 10 nm within 996 s and then increases to 12 nm at 2129 s. EDP and EELS results show that the Li crystal is covered by poorly crystallized Li_2O (Figure 2o−q). In contrast, there are many uneven bumps (island-like particles) with thicknesses varying from 12 to 70 nm on the surface of Na (Figure 2r−t). The formed small islands are gradually aggregated into large ones under O_2 exposure, according to Ostwald ripening[13] (the smaller the size, the greater the chemical potential, which is consistent with the Gibbs−Duhem relation[14−16]) with the first observation. A Kirkendall effect is also observed. In addition to Na_2O, Na_2O_2 (peroxide) with good crystallinity is found in the O-rich passivation layer detected by EDP and EELS (Figure 2u−w). In the case of N_2 exposure, there is no N-containing component but Li_2O or Na_2O is found (Figures S7 and S8). It should be noted that the oxygen species come from the tiny amount of oxygen present in the ETEM even at a very high vacuum (Figures S9 and S10). In a CO_2 atmosphere, the surfaces of Li and Na are uniformly covered by carbonates (Figures S11 and S12). Na_2CO_3 rapidly reaches a maximum

https://doi.org/10.1021/jacs.2c13589
J. Am. Chem. Soc. 2023, 145, 10576−10583

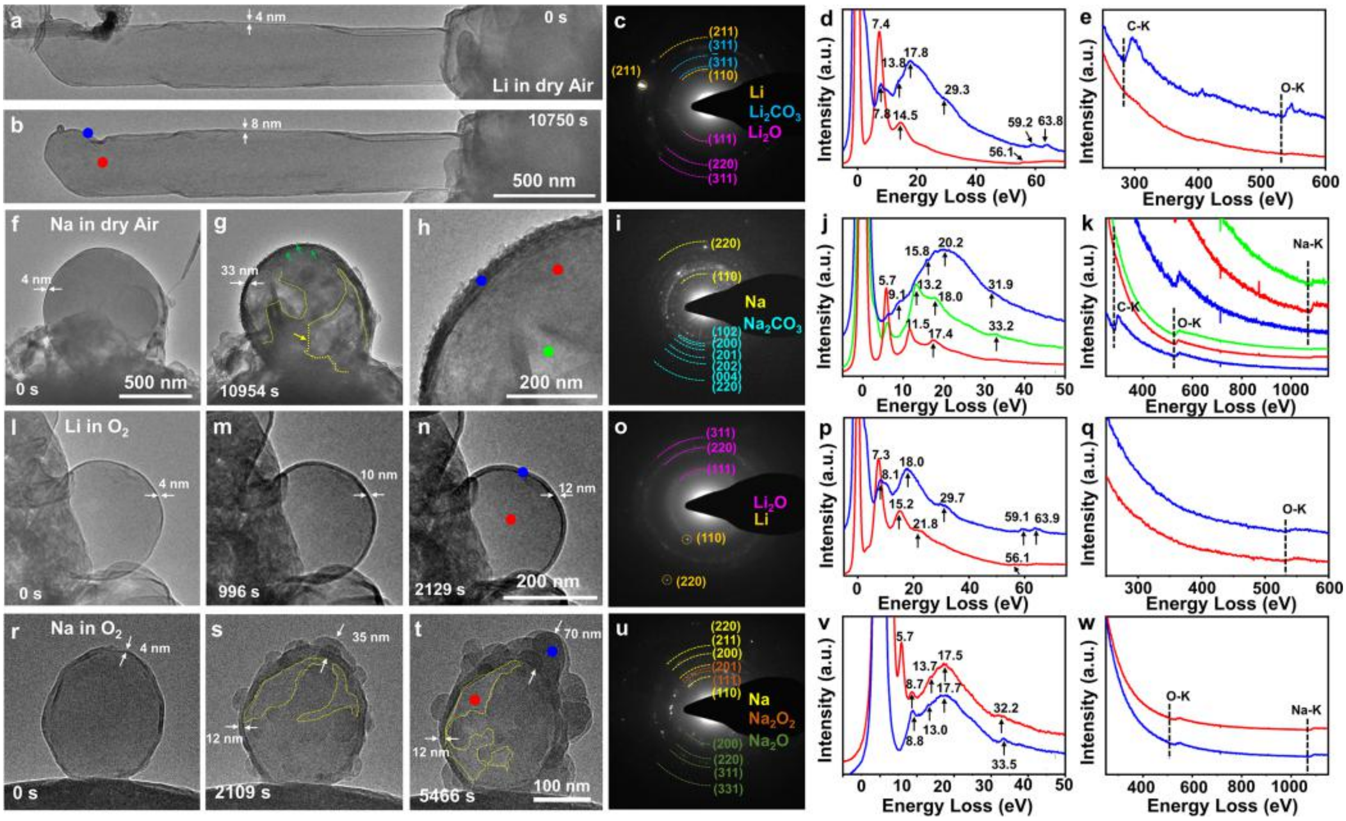

Figure 2. Nano-scale *in situ* ETEM investigation of the surface layer formation processes of Li and Na in dry air or O_2. (a, b) Time-lapse TEM images of Li in dry air. (c−e) Related EDP and EELS results taken from (b). (f−h) Time-lapse TEM images of Na in dry air. (i−k) Related EDP and EELS results taken from (h). (l−n) Time-lapse TEM images of Li in O_2. (o−q) Related EDP and EELS results taken from (n). (r−t) Time-lapse TEM images of Na in O_2. (u−w) Related EDP and EELS results taken from (t). The captured points of EELS are marked in TEM images. The arrows and numbers in TEM-EDP/EELS data indicate the identification of specific species (Supporting Information).

thickness, but the thickness of Li_2CO_3 increases. Thus, O_2 is the key factor to induce the surface differences of Li and Na.

Thermodynamic and Kinetic Calculations of the Li/Na-Dry Air Reactions. The preferential O_2-reactions are also supported by the calculations of Gibbs free energy (Tables S1 and S2), where the formation of Na_2O_2 from Na_2O is thermodynamically more favorable than that of Li_2O_2 from Li_2O. To interpret the whole phenomenon, the initial O_2 adsorption mechanism on M (Li or Na) and M_2O is investigated by density functional theory (DFT) calculations (Table S3). The most stable configurations with the lowest energy are shown in Figure 3a−d (others are in Figures S13−S17). The accompanying O−O bond cleavage of O_2 on Li suggests, as expected, much more negative adsorption energy (−10.4 eV) than that of O_2 on Li_2O (−5.5 eV). Calculations point toward a quick adsorption on Na_2O and a comparatively sluggish adsorption on Na. Obviously, the very favorable full electron transfer from Na to oxygen is kinetically not trivial. According to the calculations, O_2 adsorption on the Na(100) surface suffers a nondissociative process, indicating slightly higher adsorption energy (−3.7 eV) than that on the $Na_2O(100)$ surface (−3.8 eV). Thus, Li is the preferential adsorption matrix in the Li/Li_2O interface when O_2 attacks, but according to the calculations, such a preference is less clear in the Na system (O_2 on Na_2O may be even kinetically favored).

In addition, kinetics calculations are carried out to further understand the processes. The bond valence (BV) theory suggests that in the oxides, the activation barrier of M^+ migration is lower than that of O^{2-}, indicating that the growth of the oxide layer is enabled by M^+ migration accompanied by electron-conducting phases rather than O^{2-} migration (Figures S18 and S19). This is in line with our previous study[17] (the Li^+ transport in Li_2O has been thoroughly investigated for bulk Li_2O). At room temperature, a vacancy diffusion coefficient on the order of 10^{-13} cm^2/s with an activation energy of 0.7 eV is derived corresponding to a Li^+ diffusion coefficient of 10^{-28} cm^2/s in Li_2O with an activation energy of 1.6 eV (Supporting Information).[17] For Na_2O, no quantitative experimental results are available. Ab initio molecular dynamics (AIMD) simulation (Figures 3e,g, S20, and S21) gives a Li^+ diffusion coefficient of about 7×10^{-16} cm^2/s at 300 K. For Na_2O at the same temperature, a value of about 1×10^{-10} cm^2/s is found by modeling. It can be concluded that the Na^+ conductivity in Na_2O is higher, which needs to be further corroborated by experiments. In both bulk phases of Li_2O and Na_2O, the electronic conductivity is significantly lower and of p-type under air. Directly at the contact with the alkaline metal, the p-type conductivity is much less but the electronic conductivity might change to n-type. Even if the electronic conductivity already at the contact might be indeed higher than the ionic one, overall in the oxide, the ion conductivity will prevail and the chemical diffusion coefficient that determines oxide growth will be determined by the electronic conductivity (Supporting Information and Figure S22). It is worth noting that modeling and cryo-TEM results show that electron leakage could occur via defects, surfaces, and grain boundaries in the initial oxide products (Figure S23), indicating rather high electronic

https://doi.org/10.1021/jacs.2c13589
J. Am. Chem. Soc. 2023, 145, 10576−10583

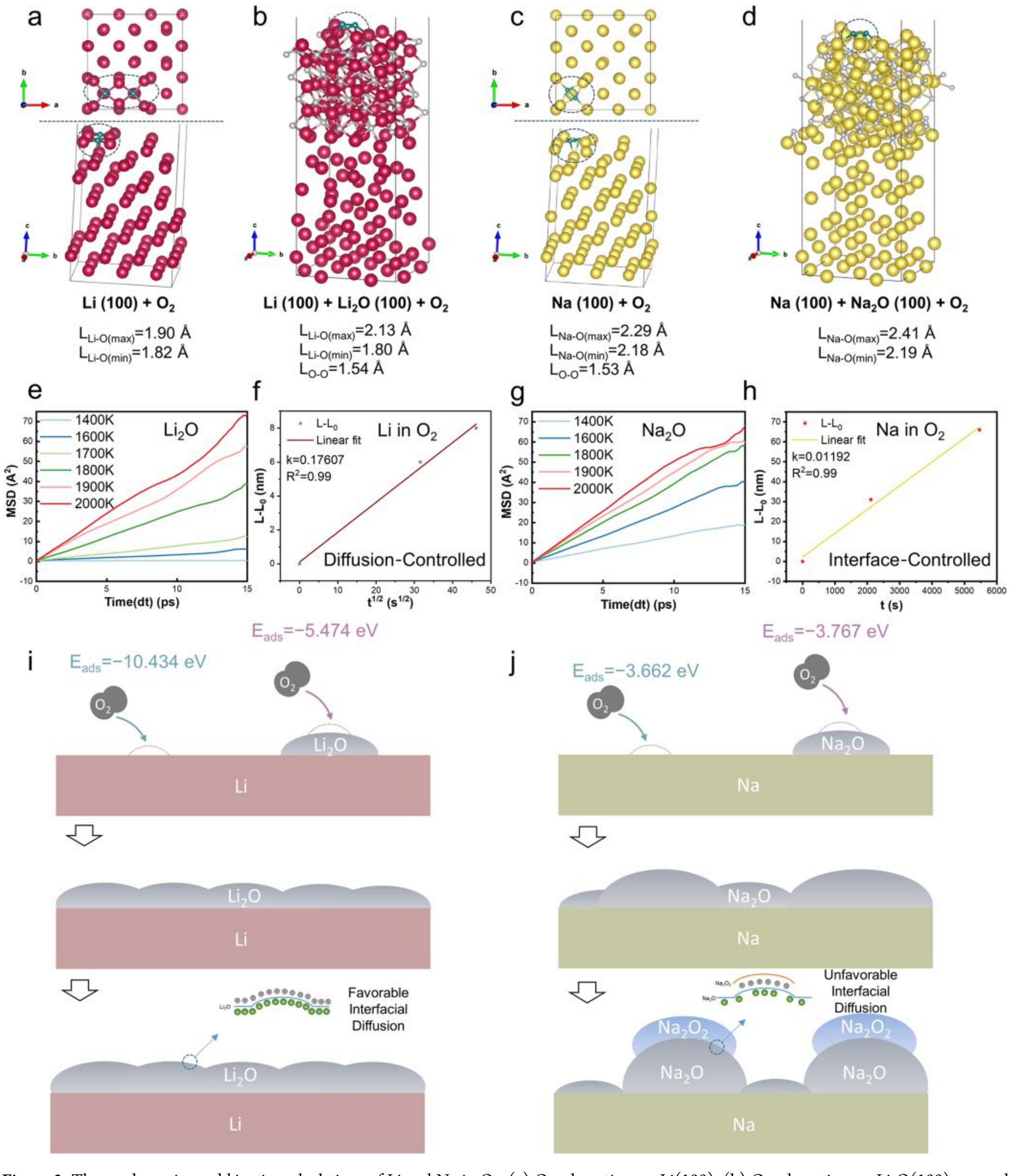

Figure 3. Thermodynamics and kinetics calculations of Li and Na in O_2. (a) O_2 adsorption on Li(100). (b) O_2 adsorption on Li_2O(100) covered on Li(100). (c) O_2 adsorption on Na(100). (d) O_2 adsorption on Na_2O(100) covered on Na(100). Note that the shown models are the ones with the lowest energy after structural relaxation. The related bonding lengths are also marked. (e, g) Mean square displacement (MSD) of ab initio molecular dynamics (AIMD) simulations for Li_2O and Na_2O at different temperatures, respectively. (f, h) Plots of the thickness increment of the passivation layer about Li and Na in O_2 versus the square root of time and time, respectively. (i, j) Schematic of passivation processes of Li and Na in O_2.

conduction for these oxides in the initial stages where they are very thin (the size of the grains usually has an influence on the conductivity[18]). Also, tunneling will then be significant, and the ion conductivity, which is higher in Na_2O, will determine the grain growth under those conditions. At any rate, the $L \propto t^{1/2}$ relationship that is found for Li_2O indicates chemical

https://doi.org/10.1021/jacs.2c13589
J. Am. Chem. Soc. 2023, 145, 10576−10583

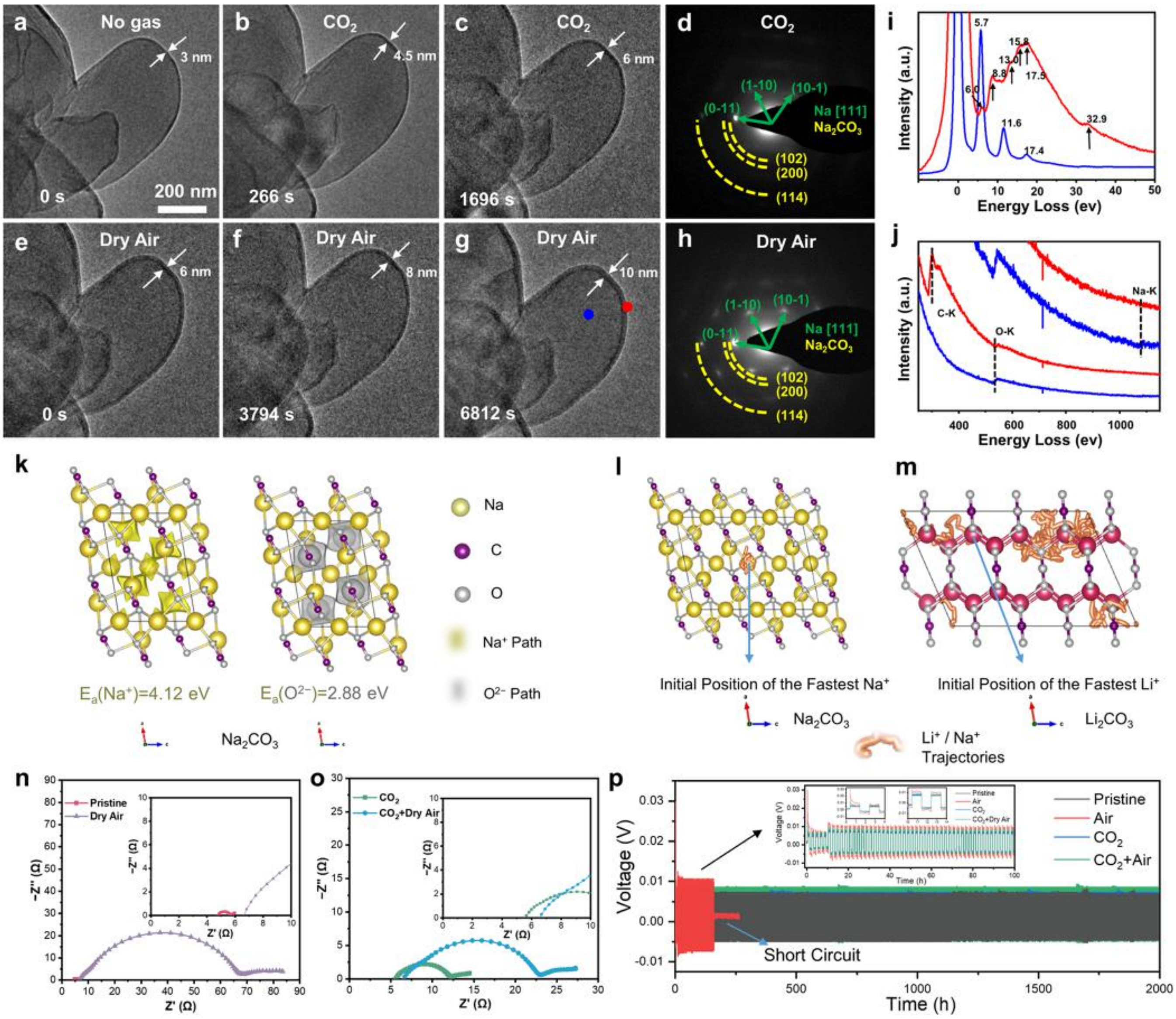

Figure 4. Carbonate prepassivation. (a−c) Time-lapse TEM images of Na in CO_2. (d) Related EDP result taken from (c). (e−g) Time-lapse TEM images of Na in dry air after CO_2 exposure. (h−j) Related EDP and EELS results taken from (g). (k) The ionic migration channels of Na_2CO_3 via the BV method. (l, m) The trajectories of Na^+ and Li^+ (the fastest ions) in Na_2CO_3 and Li_2CO_3 via the AIMD method within the time interval of 6−20 ps at T = 1200 K. (n, o) Electrochemical impedance spectroscopy (EIS) analysis of the symmetric cells based on pristine Na, dry air-treated Na, CO_2-treated Na, and CO_2- and further dry air-treated Na before cycling. (p) The cycling stability tests of the above symmetric cells at 1 mAh/cm^2.

diffusion. The growth relation is however rather a linear one in the Na_2O case and seems to reflect the sluggish interfacial processes in the Na case again.[19] In addition, the activation energies (Figures S24 and S25 and Table S4) and vacancy formation energies (Figure S26) of peroxides and oxides are also calculated via the nudged elastic band (NEB) method. It can be seen that oxygen migration is relatively easy in Na_2O_2, indicating that oxygen can pass through Na_2O_2 and further react with the inner Na_2O. Furthermore, Na migration in Na_2O_2 is more difficult than that in Na_2O (Table S5), indicating that the Na diffusion is more difficult at Na_2O/Na_2O_2 interface. Thus, there is short-range diffusion at interfaces of Na_2O and Na_2O_2 on Na with different crystallographic orientations, leading to a highly anisotropic growth of Na_2O/Na_2O_2, but amorphicity of Li_2O facilitates an isotropic Li^+ diffusion, leading to a homogeneous growth of Li_2O. Moreover, the reaction of CO_2 with Na_2O/Na_2O_2 follows an interface-controlled reaction ($L \propto t$) in Figure S27 and the reaction of CO_2 with Li_2O follows a diffusion-controlled reaction ($L \propto t^{1/2}$) in Figure S28.

After excluding mechanical factors such as the lattice mismatch between various components (Tables S6−S8), a specific reaction mechanism of Li and Na with oxygen can be proposed in Figure 3i,j. In the Li−O_2 system, after the initial O_2 adsorption on active sites such as defects, Li_2O is formed immediately. Subsequent O_2 adsorption still preferentially occurs at the fresh Li sites rather than on Li_2O, leading to the complete and compact coverage of Li_2O until no more fresh Li is present, which can also explain that N_2 does not participate in the initial reaction. Particularly, the low diffusion rate prevents the formation of thick Li_2O via mass transfer and the single product (Li_2O) also induces a uniform flux of Li

https://doi.org/10.1021/jacs.2c13589
J. Am. Chem. Soc. 2023, 145, 10576−10583

diffusion. In the case of the Na−O_2 system, the O_2 adsorption on Na and Na_2O has a similar probability, causing a relatively huge initial size distribution among different Na_2O islands. Small Na_2O islands are inclined to diffuse and merge into big islands (Ostwald Ripening) to reduce surface energy. Meanwhile, the formation of Na_2O_2 based on Na_2O can further thicken the passivation layer, and there is unfavorable interfacial diffusion through Na_2O/Na_2O_2, leading to an uneven Na_2O/Na_2O_2 growth (insufficient Na ions preferentially tend to gather on the tip, which is similar to the dendrite growth mechanism of metal[20]). Once Na_2O_2 is contacted with Na, new Na_2O will be produced (Table S2). On further exposure to CO_2, the Li system produces a uniform Li_2CO_3 based on the previous homogeneous and thin Li_2O, which makes the bulk Li stable and shiny in dry air. In contrast, the passivation layer on Na is rough and porous because the Na_2O/Na_2O_2 layer is first formed, followed by the formation of Na_2CO_3, where the newly generated O_2 from the reaction of Na_2O_2 and CO_2 may escape, leading to many voids and holes that are likely to crack owing to the Kirkendall effect. Thus, a porous passivation layer with many cracks leads to fast Na failure in dry air. Although Li^+ also moves faster than O^{2-}, there is no Kirkendall diffusion in the Li system because the thin and compact coverage of Li_2O can protect the Li metal from reacting too much with oxygen. However, there are rough and porous Na_2O/Na_2O_2 layers on the Na surface, which involves the ongoing reaction of sodium with oxygen.

Design Anticorrosive Na via Carbonate Prepassivation. In order to render Na stable in dry air, *in situ* surface treatment to introduce a protection layer before the oxidation process is a feasible strategy. For this purpose, CO_2 treatment is employed in order to produce a homogeneous Na_2CO_3 layer as seen in Figure S12 (Table S9 lists favorable kinetic parameters of CO_2 gas). *In situ* ETEM tests are designed to confirm the compactness of Na_2CO_3. When CO_2 is brought into contact with the fresh Na, a uniform and thin passivation layer (3 nm) with poor crystallinity is formed after 266 s and the film thickness only increases to 6 nm until 1696 s, as shown in Figure 4a−d. Then, the gas environment is switched from CO_2 to dry air. It is found that dry air cannot destroy the Na particle covered by Na_2CO_3 and the film thickness grows slowly and steadily to 10 nm after 6812 s without other components (Figure 4e−h,j). Moreover, the compact Na_2CO_3 can even protect Na from O_2 attack when replacing dry air with O_2 in the second step (Figure S29). To interpret this phenomenon, the BV method was conducted to confirm the higher migration barrier of Na^+ than that of O^{2-} in Na_2CO_3 (Figure 4k), which results in slow diffusion dynamics of Na^+ (electron diffusion is ignored due to the favorable conduction of concomitant carbon) and limits the further growth of Na_2CO_3. Meanwhile, the AIMD method demonstrates that Na^+ only thermally vibrates around initial locations even at 1200 K (Figure 4l), while Li hops among lattice sites (Figures 4m and S30), verifying that Na^+ migration in Na_2CO_3 follows a diffusion-controlled reaction ($L \propto t^{1/2}$) (Figure S31), while Li^+ migration in Li_2CO_3 follows an interface-controlled reaction ($L \propto t$) (Figure S32), which is completely opposite to their migration in corresponding oxides shown in Figure 3e−h. Thus, the Li−CO_2 reaction is difficult to achieve a stable state opposite to the Na−CO_2 reaction.

In order to examine the effectiveness of the above strategy, symmetric Na||Na batteries with Na treated under different conditions are assembled to analyze the electrochemical impedance at the open circuit, and the corresponding interfacial resistances (R_{SEI}) are shown in Figures 4n,o and S33. A low R_{SEI} of ∼0.5 Ω is shown for batteries with pristine Na, which drastically increases to ∼35 Ω after dry air exposure owing to the low ionic conductivity of a thick and porous passivation layer. In contrast, a much lower R_{SEI} of ∼4 Ω is observed after CO_2 passivation, which slightly increases to ∼7 Ω after further dry air attack because the Na_2CO_3 artificial SEI may be more compact than the SEI formed on bare Na. The cycling stability of these cells is compared in Figure 4p, which demonstrates clearly that the voltage polarization of cells with pristine Na is similar to that of cells with CO_2-treated Na. Cell with Na after dry air contact suffers from an unstable plating/stripping (irregular curve) process with a short circuit after only 160 h, suggesting that the rough SEI on dry air-treated Na easily induces Na dendrites (Figure S34). Instead, the other cells can achieve stable cycling with low voltage polarization and a long lifespan of over 2000 h, indicating that favorable electron/ion transport pathways in the inner layer of SEI consist of Na_2CO_3 and concomitant carbon. Differently, CO_2 seems to have a limited protection function in a Li-based system (Figures S35 and S36).

Furthermore, the K passivation behavior in O_2 is also investigated via ETEM in Figure S37, which may be induced by the formation of superoxide (KO_2). Not only the electroactive alkali metals but also Al and Cu, acting as current collector materials in rechargeable batteries, also show different behaviors in terms of air stability. Compact and even self-healing Al_2O_3 can effectively protect Al from corrosion,[21] while Cu_2O and CuO inhomogeneously spread over the surface.[22] Thus, the air stability of metals can be investigated from the aspect of the oxidation process analogous to Li and Na.

■ CONCLUSIONS

Overall, a rather comprehensive understanding of the detailed physicochemical processes of the corrosion reactions between Li/Na and dry air has been proposed on the basis of experimental characterization and theoretical simulation. Thermodynamic and kinetic differences between Li- and Na-based reactions lead to microscopic and macroscopic morphology variations, seriously affecting air stability. In this respect, this work provides a microscopic picture that is quite different from the usual explanations of the different chemical activity between Li and Na with respect to oxygen. We also suggest a strategy for improving Na surface stability: forming an appropriate artificial SEI (e.g., Na_2CO_3 formed by exposure to CO_2), which seems to solve the problem of spontaneous formation of a poor-quality oxide-based passivation layer. The growth of amorphous artificial SEI films possibly enables a denser SEI. This approach can also be extended to other kinds of energy storage, which suffer from analogous corrosion effects. The detailed analyses (crystallinities, morphology features, diffusion properties, etc.) of M_2O, M_2O_2, and M_2CO_3 also help in understanding the porosity and growth of SEI in an actual battery system toward the controllable interfacial chemistry of Li and Na.

■ ASSOCIATED CONTENT

Supporting Information

The Supporting Information is available free of charge at https://pubs.acs.org/doi/10.1021/jacs.2c13589.

https://doi.org/10.1021/jacs.2c13589
J. Am. Chem. Soc. 2023, 145, 10576−10583

Details of methods, additional characterization including cryo-TEM images, ETEM images, etc., calculation results including thermodynamics, kinetics, etc., and details of plots of additional figures and tables (PDF)

AUTHOR INFORMATION

Corresponding Authors

Yaxiang Lu − *Key Laboratory for Renewable Energy, Beijing Key Laboratory for New Energy Materials and Devices, Beijing National Laboratory for Condensed Matter Physics, Institute of Physics, Chinese Academy of Sciences, Beijing 100190, China; Huairou Division, Institute of Physics, Chinese Academy of Sciences, Beijing 101400, China; Yangtze River Delta Physics Research Center, Liyang, Jiangsu 213300, China;* orcid.org/0000-0001-5202-175X; Email: yxlu@iphy.ac.cn

Ruijuan Xiao − *Key Laboratory for Renewable Energy, Beijing Key Laboratory for New Energy Materials and Devices, Beijing National Laboratory for Condensed Matter Physics, Institute of Physics, Chinese Academy of Sciences, Beijing 100190, China; Yangtze River Delta Physics Research Center, Liyang, Jiangsu 213300, China;* orcid.org/0000-0003-0930-9576; Email: rjxiao@iphy.ac.cn

Jianyu Huang − *Clean Nano Energy Center, State Key Laboratory of Metastable Materials Science and Technology, Yanshan University, Qinhuangdao 066004, China; School of Materials Science and Engineering, Xiangtan University, Xiangtan, Hunan 411105, China;* orcid.org/0000-0002-8424-5368; Email: jyhuang8@hotmail.com

Yong-Sheng Hu − *Key Laboratory for Renewable Energy, Beijing Key Laboratory for New Energy Materials and Devices, Beijing National Laboratory for Condensed Matter Physics, Institute of Physics, Chinese Academy of Sciences, Beijing 100190, China; College of Materials Science and Optoelectronic Technology, University of Chinese Academy of Sciences, Beijing 100049, China; Huairou Division, Institute of Physics, Chinese Academy of Sciences, Beijing 101400, China; Yangtze River Delta Physics Research Center, Liyang, Jiangsu 213300, China;* orcid.org/0000-0002-8430-6474; Email: yshu@iphy.ac.cn

Authors

Yuqi Li − *Key Laboratory for Renewable Energy, Beijing Key Laboratory for New Energy Materials and Devices, Beijing National Laboratory for Condensed Matter Physics, Institute of Physics, Chinese Academy of Sciences, Beijing 100190, China; College of Materials Science and Optoelectronic Technology, University of Chinese Academy of Sciences, Beijing 100049, China;* orcid.org/0000-0003-1501-1549

Qiunan Liu − *Clean Nano Energy Center, State Key Laboratory of Metastable Materials Science and Technology, Yanshan University, Qinhuangdao 066004, China;* orcid.org/0000-0003-3684-5841

Siyuan Wu − *Key Laboratory for Renewable Energy, Beijing Key Laboratory for New Energy Materials and Devices, Beijing National Laboratory for Condensed Matter Physics, Institute of Physics, Chinese Academy of Sciences, Beijing 100190, China; College of Materials Science and Optoelectronic Technology, University of Chinese Academy of Sciences, Beijing 100049, China*

Lin Geng − *Clean Nano Energy Center, State Key Laboratory of Metastable Materials Science and Technology, Yanshan University, Qinhuangdao 066004, China*

Jelena Popovic − *Physical Chemistry of Solids, Max Planck Institute for Solid State Research, Stuttgart 70569, Germany*

Yu Li − *Key Laboratory for Renewable Energy, Beijing Key Laboratory for New Energy Materials and Devices, Beijing National Laboratory for Condensed Matter Physics, Institute of Physics, Chinese Academy of Sciences, Beijing 100190, China; College of Materials Science and Optoelectronic Technology, University of Chinese Academy of Sciences, Beijing 100049, China; Huairou Division, Institute of Physics, Chinese Academy of Sciences, Beijing 101400, China*

Zhao Chen − *Key Laboratory for Renewable Energy, Beijing Key Laboratory for New Energy Materials and Devices, Beijing National Laboratory for Condensed Matter Physics, Institute of Physics, Chinese Academy of Sciences, Beijing 100190, China; College of Materials Science and Optoelectronic Technology, University of Chinese Academy of Sciences, Beijing 100049, China*

Haibo Wang − *Key Laboratory for Renewable Energy, Beijing Key Laboratory for New Energy Materials and Devices, Beijing National Laboratory for Condensed Matter Physics, Institute of Physics, Chinese Academy of Sciences, Beijing 100190, China*

Yuqi Wang − *Key Laboratory for Renewable Energy, Beijing Key Laboratory for New Energy Materials and Devices, Beijing National Laboratory for Condensed Matter Physics, Institute of Physics, Chinese Academy of Sciences, Beijing 100190, China; College of Materials Science and Optoelectronic Technology, University of Chinese Academy of Sciences, Beijing 100049, China*

Tao Dai − *Key Laboratory for Renewable Energy, Beijing Key Laboratory for New Energy Materials and Devices, Beijing National Laboratory for Condensed Matter Physics, Institute of Physics, Chinese Academy of Sciences, Beijing 100190, China;* orcid.org/0000-0002-3111-3724

Yang Yang − *Key Laboratory for Renewable Energy, Beijing Key Laboratory for New Energy Materials and Devices, Beijing National Laboratory for Condensed Matter Physics, Institute of Physics, Chinese Academy of Sciences, Beijing 100190, China; College of Materials Science and Optoelectronic Technology, University of Chinese Academy of Sciences, Beijing 100049, China*

Haiming Sun − *Clean Nano Energy Center, State Key Laboratory of Metastable Materials Science and Technology, Yanshan University, Qinhuangdao 066004, China;* orcid.org/0000-0001-9085-500X

Liqiang Zhang − *Clean Nano Energy Center, State Key Laboratory of Metastable Materials Science and Technology, Yanshan University, Qinhuangdao 066004, China*

Yongfu Tang − *Clean Nano Energy Center, State Key Laboratory of Metastable Materials Science and Technology, Yanshan University, Qinhuangdao 066004, China;* orcid.org/0000-0002-6318-3110

Hong Li − *Key Laboratory for Renewable Energy, Beijing Key Laboratory for New Energy Materials and Devices, Beijing National Laboratory for Condensed Matter Physics, Institute of Physics, Chinese Academy of Sciences, Beijing 100190, China; College of Materials Science and Optoelectronic Technology, University of Chinese Academy of Sciences, Beijing 100049, China; Huairou Division, Institute of Physics, Chinese Academy of Sciences, Beijing 101400, China; Yangtze River Delta Physics Research Center, Liyang, Jiangsu 213300, China;* orcid.org/0000-0002-8659-086X

https://doi.org/10.1021/jacs.2c13589
J. Am. Chem. Soc. 2023, 145, 10576−10583

Liquan Chen − *Key Laboratory for Renewable Energy, Beijing Key Laboratory for New Energy Materials and Devices, Beijing National Laboratory for Condensed Matter Physics, Institute of Physics, Chinese Academy of Sciences, Beijing 100190, China*

Joachim Maier − *Physical Chemistry of Solids, Max Planck Institute for Solid State Research, Stuttgart 70569, Germany;* orcid.org/0000-0003-2274-6068

Complete contact information is available at:
https://pubs.acs.org/10.1021/jacs.2c13589

Author Contributions

[○]Y.L. and Q.L. contributed equally to this work.

Notes

The authors declare no competing financial interest.

■ ACKNOWLEDGMENTS

This work was supported by the National Key Technologies R&D Program of China (2022YFB2402500), National Natural Science Foundation of China (52122214, 52072403, 21935009, and U20A20336), Youth Innovation Promotion Association, Chinese Academy of Sciences (2020006), and Natural Science Foundation of Hebei Province (Nos. B2020203037).

■ REFERENCES

(1) Goodenough, J. B.; Park, K.-S. The Li-Ion Rechargeable Battery: A Perspective. *J. Am. Chem. Soc.* **2013**, *135*, 1167−1176.

(2) Li, Y.; Lu, Y.; Adelhelm, P.; Titirici, M.-M.; Hu, Y.-S. Intercalation chemistry of graphite: alkali metal ions and beyond. *Chem. Soc. Rev.* **2019**, *48*, 4655−4687.

(3) Cheng, X.-B.; Zhang, R.; Zhao, C.-Z.; Zhang, Q. Toward safe lithium metal anode in rechargeable batteries: a review. *Chem. Rev.* **2017**, *117*, 10403−10473.

(4) Li, Y.; Li, Y.; Sun, Y.; Butz, B.; Yan, K.; Koh, A. L.; Zhao, J.; Pei, A.; Cui, Y. Revealing Nanoscale Passivation and Corrosion Mechanisms of Reactive Battery Materials in Gas Environments. *Nano Lett.* **2017**, *17*, 5171−5178.

(5) Shen, X.; Li, Y.; Qian, T.; Liu, J.; Zhou, J.; Yan, C.; Goodenough, J. B. Lithium anode stable in air for low-cost fabrication of a dendrite-free lithium battery. *Nat. Commun.* **2019**, *10*, No. 900.

(6) Duffner, F.; Kronemeyer, N.; Tübke, J.; Leker, J.; Winter, M.; Schmuch, R. Post-lithium-ion battery cell production and its compatibility with lithium-ion cell production infrastructure. *Nat. Energy* **2021**, *6*, 123−134.

(7) Lee, B.; Paek, E.; Mitlin, D.; Lee, S. W. Sodium metal anodes: Emerging solutions to dendrite growth. *Chem. Rev.* **2019**, *119*, 5416−5460.

(8) Herrington, B. L. The Reaction of Sodium with Dry Oxygen. *J. Phys. Chem. A* **1934**, *38*, 675−682.

(9) Mason, P. E.; Uhlig, F.; Vaněk, V.; Buttersack, T.; Bauerecker, S.; Jungwirth, P. Coulomb explosion during the early stages of the reaction of alkali metals with water. *Nat. Chem.* **2015**, *7*, 250−254.

(10) Asadi, M.; Sayahpour, B.; Abbasi, P.; Ngo, A. T.; Karis, K.; Jokisaari, J. R.; Liu, C.; Narayanan, B.; Gerard, M.; Yasaei, P.; et al. A lithium−oxygen battery with a long cycle life in an air-like atmosphere. *Nature* **2018**, *555*, 502−506.

(11) Cheng, Y.; Zhang, L.; Zhang, Q.; Li, J.; Tang, Y.; Delmas, C.; Zhu, T.; Winter, M.; Wang, M.-S.; Huang, J. Understanding all solid-state lithium batteries through in situ transmission electron microscopy. *Mater. Today* **2021**, *42*, 137−161.

(12) Sun, Y.; Zuo, X.; Sankaranarayanan, S. K.; Peng, S.; Narayanan, B.; Kamath, G. Quantitative 3D evolution of colloidal nanoparticle oxidation in solution. *Science* **2017**, *356*, 303−307.

(13) Kolthoff, I. M. Perfection and agglomeration of crystalline precipitates on aging. *Science* **1936**, *84*, 376−377.

(14) Li, C.-Y.; Blakely, J. M.; Feingold, A. H. Mass transport analysis for ostwald ripening and related phenomena. *Acta Metall.* **1966**, *14*, 1397−1402.

(15) Nauman, E. B.; He, D. Q. Nonlinear diffusion and phase separation. *Chem. Eng. Sci.* **2001**, *56*, 1999−2018.

(16) Watanabe, H.; Suzuki, M.; Inaoka, H.; Ito, N. Ostwald ripening in multiple-bubble nuclei. *J. Chem. Phys.* **2014**, *141*, No. 234703.

(17) Lorger, S.; Usiskin, R.; Maier, J. Transport and Charge Carrier Chemistry in Lithium Oxide. *J. Electrochem. Soc.* **2019**, *166*, A2215−A2220.

(18) Prutsch, D.; Breuer, S.; Uitz, M.; Bottke, P.; Langer, J.; Lunghammer, S.; Philipp, M.; Posch, P.; Pregartner, V.; Stanje, B.; Dunst, A.; Wohlmuth, D.; Brandstätter, H.; Schmidt, W.; Epp, V.; Chadwick, A.; Hanzu, I.; Wilkening, M. Nanostructured Ceramics: Ionic Transport and Electrochemical Activity. *Z. Phys. Chem.* **2017**, *231*, 1361−1405.

(19) Choi, Y.-S.; Scanlon, D. O.; Lee, J.-C. Extending the Performance Limit of Anodes: Insights from Diffusion Kinetics of Alloying Anodes. *Adv. Energy Mater.* **2021**, *11*, No. 2003078.

(20) Chen, X.-R.; Yao, Y.-X.; Yan, C.; Zhang, R.; Cheng, X.-B.; Zhang, Q. A Diffusion−Reaction Competition Mechanism to Tailor Lithium Deposition for Lithium-Metal Batteries. *Angew. Chem., Int. Ed.* **2020**, *59*, 7743−7747.

(21) Yang, Y.; Kushima, A.; Han, W.; Xin, H.; Li, J. Liquid-like, self-healing aluminum oxide during deformation at room temperature. *Nano Lett.* **2018**, *18*, 2492−2497.

(22) Peng, J.; Chen, B.; Wang, Z.; Guo, J.; Wu, B.; Hao, S.; Zhang, Q.; Gu, L.; Zhou, Q.; Liu, Z.; et al. Surface coordination layer passivates oxidation of copper. *Nature* **2020**, *586*, 390−394.